JOURNAL OF GEOPHYSICAL RESEARCH, VOL. 96, NO. B5, PAGES 7933–7945, MAY 10, 1991

The Chemical Composition of the Dust-Free Martian Atmosphere: Preliminary Results of a Two-Dimensional Model

D. MOREAU AND L. W. ESPOSITO

Laboratory for Atmospheric and Space Physics, University of Colorado, Boulder

G. BRASSEUR

National Center for Atmospheric Research, Boulder, Colorado

This paper describes a two-dimensional model of the Martian atmosphere, in which chemical, radiative and dynamical processes are treated interactively. The model is developed for a carbon dioxide-hydrogen-oxygen-nitrogen atmosphere and provides estimates of concentrations for 19 chemical species. The dynamical equations are expressed in the transformed Eulerian coordinates. The wave driving and eddy mixing coefficients resulting from gravity and Rossby wave absorption are computed consistently with the evolving distribution of the mean zonal wind. The net diabatic heating/cooling rate is derived from a detailed radiative scheme including the contributions of CO_2, O_3, H_2O and O_2, and is computed consistently with the calculated distribution of temperature and trace species quantities. The computed temperature field as well as the meridional and seasonal variations of ozone column abundance are in good agreement with the distributions observed by Mariner 9 and Viking spacecrafts and the results obtained by previous studies. The present version of the model does not include the effects of dust, clouds and polar hood and only the chemistry in a dust-free atmosphere is considered.

INTRODUCTION

The Martian atmosphere consists mainly of CO_2 with trace quantities of N_2, Ar, O_2 and CO and other less abundant species. Carbon dioxide was first detected by *Kuiper* [1947, 1952], carbon monoxide by *Kaplan et al.* [1969] and *Connes et al.* [1969], and oxygen by *Carleton and Traub* [1972] and *Barker* [1972]. Argon and nitrogen were observed more recently by the mass spectrometer on board Viking 1 [*Nier et al.*, 1976; *Owen and Biemann*, 1976]. The mean mixing ratios derived from these observations are listed in Table 1. In the past, one-dimensional chemical models have been developed to determine the expected vertical profiles of atmospheric trace compounds in the Martian atmosphere [*Hunten and McElroy*, 1970; *Parkinson and Hunten*, 1972; *McElroy and Donahue*, 1972; *Yung et al.*, 1977; *Krasnopolsky*, 1979; *Lindner*, 1988]. These models have provided an estimate of the mean concentration of these gases as a function of height and have emphasized the role of water vapor in the ozone budget. They do not, however, account for the effects of meridional transport nor for the latitudinal and seasonal variation of solar insolation. Two-dimensional models provide a better description of these processes and include a more detailed formulation of mass, momentum and energy transport.

In the past 20 years, data have become available to test the theory of atmospheric dynamics and to understand the thermal structure of the Martian atmosphere. These data are important to estimate the strength of the meridional transport of trace gases. Dynamics on Mars is mainly forced by differential heating associated with solar absorption, by mass flux produced by the seasonal condensation and sublimation of CO_2 at the polar cap and the momentum deposition associated with the absorption of tides, gravity and planetary waves. Model simulations of the Martian circulation [*Gierasch and Goody*, 1968; *Leovy and Mintz*, 1969; *Pollack et al.*, 1976; *Pollack et al.*, 1981; *Haberle et al.*, 1982; *Schneider*, 1983; *Magalhaes*, 1987] are generally consistent with the basic features observed, such as the temperature structure.

The purpose of the present paper is to describe a two-dimensional model of the Martian atmosphere formulated in the transformed Eulerian coordinates, in which chemical, radiative and dynamical processes are treated interactively. The model includes a detailed radiative scheme which derives the diabatic heating rate consistently with calculated distribution of temperature and trace species densities. The calculation of the dynamics is performed above 6 km altitude, where a forcing assumed to represent the influence of topography is applied. Eddy diffusivity is included in the thermodynamic and trace species continuity equations to account for transient and dissipative processes. Calculated wave driving and eddy mixing coefficients resulting from gravity and Rossby wave absorption vary with the evolving mean zonal wind.

MODEL DESCRIPTION

The present model is an adaptation for the Martian conditions of the model developed earlier for the terrestrial atmosphere by *Brasseur et al.* [1990]. It extends from pole to pole with a latitudinal resolution of 5 degrees and from the surface to 85 km altitude with a vertical resolution of 1 km.

Radiation

The net diabatic heating rate is computed below 40 km using the detailed radiative code of the National Center for

Paper number 90JB02544.
0148-0227/91/90JB-02544$05.00

TABLE 1. Atmospheric Composition of Mars

Constituent	Percent
CO_2	95.32
N_2	2.70
Ar	1.50
O_2	0.13
CO	0.07

Atmospheric Research (NCAR) Community Climate Model [*Kiehl et al.*, 1987], adapted for the Martian conditions. This code includes the radiative effects of CO_2, O_3, H_2O and O_2. The contribution of carbon dioxide in the near infrared is calculated following the formulation of *Sasamori et al.* [1972]; the effect of water vapor in the near infrared is derived from the parameterization of *Kratz and Cess* [1985] for the direct beam and the formulation of *Lacis and Hansen* [1974] for the reflected beam. The contribution of ozone in the ultraviolet and visible is computed following *Lacis and Hansen* [1974]. Finally, the effect of oxygen is derived from the parameterization of *Kiehl and Yamamouchi* [1985]. The radiative transfer equations are solved for two large spectral regions: 0–0.9 µm and 0.9–4.0 µm, respectively. Above 40 km altitude where the conditions depart significantly from local-thermodynamical equilibrium, the cooling rate is computed using a Newtonian cooling formulation [*Dickinson*, 1972]. Thus in this part of the atmosphere, radiative exchange is assumed to occur between a given atmospheric layer and the upper boundary of the atmosphere. The 24-hour average of the solar heating rate is approximated by a 4-point integral between sunrise and sunset. The same method is used to provide the diurnal average of the photodissociation coefficients. In the present version of the model, the radiative effects of clouds, polar hood and dust are ignored.

Chemistry

The chemical model of the Martian atmosphere is developed to study a CO_2—H_2O—N_2 atmosphere. It includes the calculation of the meridional distributions of CO_2, O_2, CO, O, $O(^1D)$, O_3, H_2, H, OH, HO_2, N, NO, N_2, NO_2, NO_3, N_2O_5, HNO_2, HNO_3, and N_2O. The distribution of long-lived species (CO_2, CO, O_2, H_2, N_2O) or of chemical families ($O_x = O_3 + O(^3P) + O(^1D)$; $NO_y = N + NO + NO_2 + NO_3 + 2N_2O_5 + HNO_2 + HNO_3$; $HO_x = H + OH + HO_2 + 2H_2O_2$) is derived by solving for each of them a continuity/transport equation. For the fast-reacting species, photochemical equilibrium conditions are assumed. Listed in Tables 2*a* and 2*b* are the chemical reactions introduced in the model. Most of the rates adopted are taken from the Jet Propulsion Laboratory (JPL) 1987 compilation [*DeMore et al.*, 1987]. The rates of reactions 38 and 40 to 46 are from *McConnell and McElroy* [1973]. In order to account for the higher efficiency of the three-body reactions when CO_2, as opposed to a mixture of N_2, O_2 and Ar, acts as the third body M, the rate constants given in Table 2*b* are multiplied by a factor of 2. The choice of this factor is based on studies of the $O + O_2 + M$ reaction performed for M = CO_2, N_2, Ar, etc. [e.g., *Kaufman and Kelso*, 1967; *Hogan and Burch*, 1976] and is used as working values for all three-body reactions. Photodissociation processes included in the model are tabulated in Table 2*c*. The absorption cross sections used in this work are very similar to those presented in the JPL 1987 compilation. In the case of CO_2, our values are taken from *Shemansky* [1972] and *Lewis and Carver* [1983]. Due to the strong temperature dependence of CO_2 cross sections and to account for the low Martian atmospheric temperature, these cross sections have been adapted as proposed by *Lewis and Carver* [1983]. The values of the solar irradiance are taken from *Brasseur and Simon* [1981] and scaled for Martian conditions. The boundary conditions applied at the surface and at 85 km altitude for the different species or families are given in Table 3.

In the Martian atmosphere the behavior of ozone is mainly controlled by the amount of atmospheric water vapor. Moreover, water vapor is the primary source of the odd hydrogen species which play an essential role in ozone destruction, as well as in the recombination of CO into CO_2 [*McElroy and Donahue*, 1972; *Parkinson and Hunten*, 1972]. Some observations have shown a strong anticorrelation between water vapor and ozone concentrations [e.g., *Barth*, 1985]. They suggest that ozone reaches high concentrations where the concentration of water is reduced to its minimum value by the effect of condensation on the surface. Consequently, they argue that ozone could play an important radiative role in the winter polar atmosphere. Typical ozone abundances in the winter polar atmosphere can provide significant heating and hence affect CO_2 and H_2O condensation processes. To obtain an accurate representation of the atmospheric chemistry, it is necessary to accurately specify or determine the water vapor distribution. Observations have shown that a seasonal exchange of water takes place with nonatmospheric reservoirs. These include surface and subsurface ice, water ice on/or within the polar caps and adsorbed water in the regolith. As the model does not yet include a consistent representation of the water cycle, different water vapor distributions will be considered, with column values being consistent with the observed data of the MAWD experiment on Viking [*Farmer et al.*, 1977; *Jakosky and Farmer*, 1982] and of Mariner 9 [*Hanel et al.*, 1972; *Conrath et al.*, 1973].

Due to the very low Martian atmospheric temperatures, especially in the winter polar regions, condensation of H_2O_2 may also occur and affect the odd hydrogen chemistry. From the analysis of thermodynamical data, the H_2O_2 vapor partial pressure (p) below 220 K is prescribed by the following expression [*Lindner*, 1988]

$$\log(p)=11.98 - (3422/T) \tag{1}$$

where p and T are expressed in millimeters Hg and K, respectively. The calculated number densities for H_2O_2 are constrained to lie at or below the local saturation number density.

Dynamics

The dynamical and transport formulation used in the model is similar to that used by *Brasseur et al.* [1990]. The entropy (potential temperature) and the chemical species are advected by a residual (transformed Eulerian) mean meridional circulation [*Andrews and McIntyre*, 1976; *Boyd*, 1976], which is forced by wave driving. Since a detailed treatment of the dynamics in the lower atmosphere cannot be properly achieved by a two-dimensional model, especially due to the complex topography of Mars, the meridional circulation has been calculated only above 6 km altitude. At this level a boundary condition on the vertical velocity is applied. Below 6 km, the stream function is linearly extrapolated to reach zero at the surface. Sources of momentum and eddy diffusion result from

TABLE 2*a*. Two-Body Reactions Introduced in the Model

Reaction			Rate, cm^{-3} s^{-1}	Reaction Number
$O + O_3$	$\rightarrow$	$2O_2$	8.0e-12 exp(-2060/T)	1
$N_2 + O(^1D)$	$\rightarrow$	$O + N_2$	1.8e-11 exp(110/T)	2
$CO_2 + O(^1D)$	$\rightarrow$	$O + CO_2$	7.4e-11 exp(120/T)	3
$O_3 + O(^1D)$	$\rightarrow$	$2O_2$	1.2e-10	4
$O_3 + O(^1D)$	$\rightarrow$	$O_2 + 2O$	1.2e-10	5
$CO + O(^1D)$	$\rightarrow$	$O + CO$	4.0e-11	6
$O_2 + O(^1D)$	$\rightarrow$	$O + O_2$	3.2e-11 exp(70/T)	7
$Ar + O(^1D)$	$\rightarrow$	$O + Ar$	3.0e-13	8
$O_3 + H$	$\rightarrow$	$O_2 + OH$	1.4e-10 exp(-470/T)	9
$O + OH$	$\rightarrow$	$O_2 + H$	2.2e-11 exp(120/T)	10
$O_3 + OH$	$\rightarrow$	$HO_2 + O_2$	1.6e-12 exp(-940/T)	11
$O_3 + HO_2$	$\rightarrow$	$2O_2 + OH$	1.1e-14 exp(-500/T)	12
$HO_2 + O$	$\rightarrow$	$O_2 + OH$	3.0e-11 exp(200/T)	13
$OH + OH$	$\rightarrow$	$H_2O + O$	4.2e-12 exp(-242/T)	14
$HO_2 + OH$	$\rightarrow$	$H_2O + O_2$	4.6e-11 exp(230/T)	15
$H_2 + OH$	$\rightarrow$	$H_2O + H$	5.5e-12 exp(-2000/T)	16
$H + HO_2$	$\rightarrow$	$2OH$	4.2e-10 exp(-950/T)	17
$H + HO_2$	$\rightarrow$	$H_2 + O_2$	4.2e-11 exp(-350/T)	18
$H + HO_2$	$\rightarrow$	$H_2O + O$	8.3e-11 exp(-500/T)	19
$H_2 + O$	$\rightarrow$	$OH + H$	8.8e-12 exp(-4200/T)	20
$HO_2 + HO_2$	$\rightarrow$	$H_2O_2 + O_2$	2.3e-13 exp(600/T)	21
$OH + H_2O_2$	$\rightarrow$	$H_2O + HO_2$	3.3e-12 exp(-200/T)	22
$OH + CO$	$\rightarrow$	$CO_2 + H$	1.5e-13(0.6*P+1)	23
$H_2O_2 + O$	$\rightarrow$	$HO_2 + OH$	1.4e-12 exp(-2000/T)	24
$H_2O + O(^1D)$	$\rightarrow$	$2OH$	2.2e-10	25
$H_2 + O(^1D)$	$\rightarrow$	$OH + H$	1.0e-10	26
$NO_2 + O$	$\rightarrow$	$NO + O_2$	6.5e-12 exp(120/T)	27
$NO + O_3$	$\rightarrow$	$NO_2 + O_2$	2.0e-12 exp(-1400/T)	28
$N + NO$	$\rightarrow$	$N_2 + O$	3.4e-11	29
$NO_2 + O_3$	$\rightarrow$	$NO_3 + O_2$	1.1e-13 exp(-2500/T)	30
$HNO_3 + OH$	$\rightarrow$	$H_2O + NO_3$	7.2e-15 exp(785/T)	31
$NO + HO_2$	$\rightarrow$	$OH + NO_2$	3.7e-12 exp(240/T)	32
$N_2O + O(^1D)$	$\rightarrow$	$N_2 + O_2$	4.9e-11	33
$N_2O + O(^1D)$	$\rightarrow$	$2NO$	6.7e-11	34
$N + O_2$	$\rightarrow$	$NO + O$	4.1e-12 exp(-3200/T)	35
$NO_3 + O$	$\rightarrow$	$NO_2 + O_2$	1.0e-11	36
$NO_3 + NO$	$\rightarrow$	$2NO_2$	1.7e-11 exp(150/T)	37
$N + OH$	$\rightarrow$	$NO + H$	6.8e-11	38
$N + O_3$	$\rightarrow$	$NO + O_2$	1.0e-15	39
$HNO_2 + O$	$\rightarrow$	$NO_2 + OH$	1.6e-11 exp(-1860/T)	40
$N + NO_2$	$\rightarrow$	$N_2O + O$	7.9e-12	41
$N + NO_2$	$\rightarrow$	$2NO$	6.1e-12	42
$HNO_2 + OH$	$\rightarrow$	$H_2O + NO_2$	5.0e-13	43
$HNO_3 + O$	$\rightarrow$	$OH + NO_3$	1.0e-11 exp(-1860/T)	44
$HNO_3 + H$	$\rightarrow$	$H_2 + NO_3$	1.0e-12 exp(-1180/T)	45
$HNO_3 + H$	$\rightarrow$	$OH + HNO_2$	1.0e-11 exp(-1180/T)	46

T in K and P in atmospheres; for e-12, read 10^{-12}.

TABLE 2*b*. Three-Body Reactions Adopted From the JPL 1987 Compilation

Reaction			Rate	Reaction Number
$O+O+M$	→	O_2+M	4.7e-33(300./T)$^{2.0}$ M	47
$O+O_2+M$	→	O_3+M	6.0e-34(300./T)$^{2.3}$ M	48
$CO+O+M$	→	CO_2+M	9.8e-33(-2180./T) M	49
$OH+OH+M$	→	H_2O_2+M	k_o = 6.9e-31(T/300)$^{-0.8}$	50
			k_∞ = 1.0e-11	
$H+H+M$	→	H_2+M	1.9e-32M	51
$N_2+O(^1D)+M$	→	N_2O+M	3.5e-37(T/300)$^{-0.6}$ M	52
$H+O_2+M$	→	HO_2+M	k_o = 5.7e-32(T/300)$^{-1.6}$	53
			k_∞ = 7.5e-11	
NO_2+NO_3+M	→	N_2O_5+M	k_o = 2.2e30(T/300)$^{-4.3}$	54
			k_∞ = 1.5e-12(T/300)$^{-0.5}$	
N_2O_5+M	→	NO_2+NO_3+M	2.2e-5exp(-9700/T) M	55
$NO+O+M$	→	NO_2+M	k_o = 9.0e-32(T/300)$^{-1.5}$	56
			k_∞ = 3.0e-11	
NO_2+O+M	→	NO_3+M	k_o = 9.0e-32(T/300)$^{-2.0}$	57
			k_∞ = 2.2e-11	
NO_2+OH+M	→	HNO_3+M	k_o = 2.6e-30(T/300)$^{-3.2}$	58
			k_∞ = 2.4e-11(T/300)$^{-1.3}$	
$NO+OH+M$	→	HNO_2+M	k_o = 7.0e-31(T/300)$^{-2.6}$	59
			k_∞ = 1.5e-11(T/300)$^{-0.5}$	

The values listed in this table for M = N_2 and O_2 have been multiplied by 2 to account for the higher efficiency when the third body is CO_2. See text for discussion. See *DeMore et al.* [1987] for the JPL 1987 compilation. K = $(k_o{*}M)/(1+(k_o{*}M/k_\infty))*0.6^{(1-(\log(k_o*M/k_\infty))^{-1}}$

TABLE 2*c*. Photodissociation Processes Introduced in the Model

Reaction			Wavelength Interval	Reaction Number
$O_2+h\nu$	→	$O+O$	175–245 nm	1
$O_2+h\nu$	→	$O+O(^1D)$	135–175 nm	2
$O_3+h\nu$	→	O_2+O	> 320 nm	3
$O_3+h\nu$	→	$O_2+O(^1D)$	135–320 nm	4
$H_2O+h\nu$	→	$H+OH$	135–205 nm	5
$N_2O+h\nu$	→	$N_2+O(^1D)$		6
$CO_2+h\nu$	→	$CO+O$	170–220 nm	7
$CO_2+h\nu$	→	$CO+O(^1D)$	135–170 nm	8
$NO+h\nu$	→	$N+O$		9
$H_2O_2+h\nu$	→	$2OH$	135–375 nm	10
$NO_2+h\nu$	→	$NO+O$		11
$HO_2+h\nu$	→	$O+OH$	190–225 nm	12
$N_2O_5+h\nu$	→	NO_2+NO_3		13
$HNO_3+h\nu$	→	NO_2+OH		14
$HNO_2+h\nu$	→	$NO+OH$		15
$NO_3+h\nu$	→	$NO+O_2$		16
$H_2+h\nu$	→	$2H$		17

TABLE 3. Boundary Conditions

	Flux	Mixing Ratio
	Upper Boundary	
O_x	0.	
NO_x		10 ppbv
N_2O	0.	
CO_2	0.	
CO	0.	
N_2	0.	
O_2	0.	
H_2	0.	
	Lower Boundary	
O_x	0.	
NO_x		5.9 ppbv*
N_2O		1.1 pptv*
CO_2		0.9532
CO		0.0007
N_2		0.0270
O_2		0.0013
H_2		20 ppmv

*Based on Yung et al. [1977].

the absorption of tides, gravity waves and Rossby waves. The contribution of the gravity waves is computed following the scheme proposed by *Lindzen* [1981] and *Holton* [1982]. Figure 1 shows the meridional distribution of the vertical eddy diffusion calculated for a Prandtl number $Pr = 3$ and a solar longitude $L_s = 351°$. The calculation of momentum deposition rate and the meridional eddy diffusivities associated with the absorption of planetary waves is performed following the scheme formulated by *Hitchman and Brasseur* [1988] adapted for Mars.

Surface Model

The surface temperature is calculated from an energy balance equation applied at the surface:

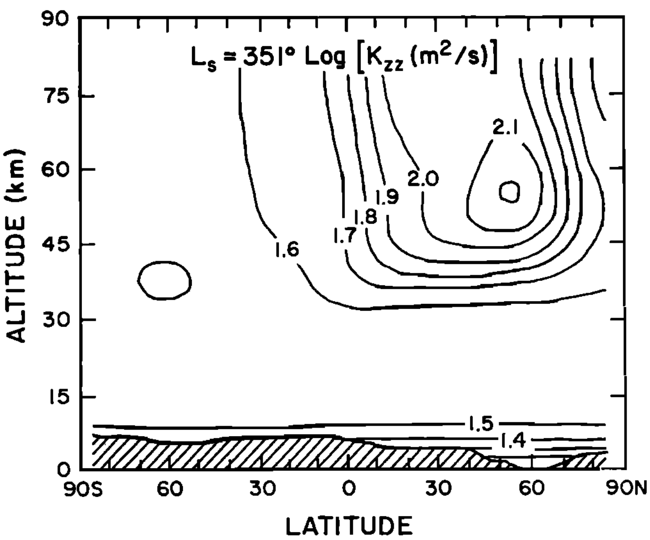

Fig. 1. Meridional distribution of the vertical eddy diffusion coefficient calculated for a solar longitude equal to 351°.

$$F_s + F_{ar} + F_c + F_{cv} + F_{cl} - \varepsilon\sigma T_s^4 = 0 \qquad (2)$$

where F_s is the rate of solar irradiance absorbed by the surface, F_{ar} the rate of thermal radiation reaching the surface, F_{cv} the heat transported by the atmosphere to the surface, F_c the rate of heat conduction into the soil, F_{cl} the rate of latent heat of condensation of CO_2, ε the emissivity of the surface, σ the Stefan-Boltzmann constant, and T_s the surface temperature. The first two terms in this equation are computed by the atmospheric radiative code described earlier. The rate of heat conduction into the soil, is computed as a function of the latitude (ϕ) by the parameterization of *Briggs* [1974]:

$$F_C = 9.3 \sin^2(\phi) \qquad (3)$$

$$F_C = 1.4 + 2.7 \cos(\phi) \qquad (4)$$

where (3) describes the heating rate in cal cm^{-2} d^{-1} before the cap formation and (4) after the cap condensation. The heat transport by the atmosphere to the surface is described by the empirical bulk transfer law (*Briggs*, 1974):

$$F_{cv} = \rho C_p C_d V [T_a - T_c] \qquad (5)$$

where ρ is the atmospheric density at the surface, C_p the specific heat at constant pressure of the atmosphere, C_d the drag coefficient, V the wind velocity at the surface, T_a the atmospheric temperature, and T_c the condensation temperature. The rate of latent heat of condensation/sublimation is given by [*Briggs*, 1974]

$$F_{cl} = M_{CO_2} LH \qquad (6)$$

where M_{CO_2} is the mass of CO_2 which condenses or sublimes, and *LH* the latent heat of CO_2 condensation. Condensation of CO_2 at the surface occurs when the heating rate of the ground is less than the infrared cooling of the surface $\varepsilon\sigma T_c^4$, where T_c is the frost temperature for CO_2.

Adopted Parameter Values

Table 4 gives the values of the parameters used in the model. The condensation temperature of CO_2 as a function of the pressure [*James and North*, 1982] is approximated by

$$T_c = 149.2 + 6.48 \ln(0.135P) \qquad (7)$$

where *P* is the surface pressure expressed in millibar. A value of 0.242 is adopted for the bolometric albedo of the ice-free ground. When the condensation of the polar cap begins, the albedo of this cap is assumed to grow linearly to a maximum value of 0.65. This limit is reached when the amount of CO_2 ice is equal to 5 g cm^{-2}. For the retreating polar cap, the albedo value is assumed to decrease linearly to its free ice value, when the amount of the CO_2 ice on the ground becomes less than 50 g cm^{-2}.

MODEL RESULTS AND DISCUSSION

The model provides a large amount of output for different times of the year, and therefore only selected results (primarily for solstice and equinox conditions) will be presented and discussed. Additional results will be given in subsequent papers in which specific problems, such as the chemical and radiative effects of the dust will be considered.

Surface Temperature

The treatment of radiative transfer in the atmosphere requires that the surface albedo and the surface temperature be

TABLE 4. Parameter Values Adopted in the Model

Parameter	Value
Radius of Mars	3.38 10^6 m
Gravitational acceleration	3.72 m s^{-2}
Gas constant	1.91 10^5 J/kg/K
Mean surface pressure	6.1 mbar
Soil albedo	0.242
Polar cap albedo	0.6 (retreating)/0.65 (prograding)
Sideral rotation frequency	7.088 10^{-5} s
Emissivity of the ground	0.95
Specific heat	840 J/K/kg
Latent heat of condensation for CO_2	5.902 10^5 J/kg
Drag coefficient	9 10^{-4}

accurately known. It is therefore important to predict the presence of the polar caps and the seasonal variation of their latitudinal extent. A detailed calculation of these parameters, based on the surface model described above, has to take into account the effect of the orbital eccentricity of Mars (0.09337) and hence of the difference in the solar insolation reaching each hemisphere. Figure 2 shows for four selected latitudes (35°S, 35°N, 65°S, 65°N) calculated surface temperatures as a function of solar longitude which are compared to a study by *Kieffer et al.* [1977]. (The aerocentric longitude of the Sun (L_s) is a seasonal index; L_s = 0 corresponds to northern spring equinox and L_s = 270 to the autumnal equinox.) The present model reproduces the values of Kieffer both at mid and at high latitudes and simulates at 65° the presence of a CO_2 ice cap in winter. Figure 3 presents the regression curve of the southern polar cap as a function of solar longitude, as generated by the model. Superimposed on this curve is the maximum extent of the south polar cap over 20 years [*James and Lumme*, 1982]. The calculated extent of the polar cap is in fairly good agreement with the observed values. The model, however, predicts a complete and instantaneous sublimation of the CO_2 cap at solar longitude of 275° while the observations made by the Viking orbiter indicate that a small permanent CO_2 cap remains over the south pole in summer [*Kieffer*, 1979]. This

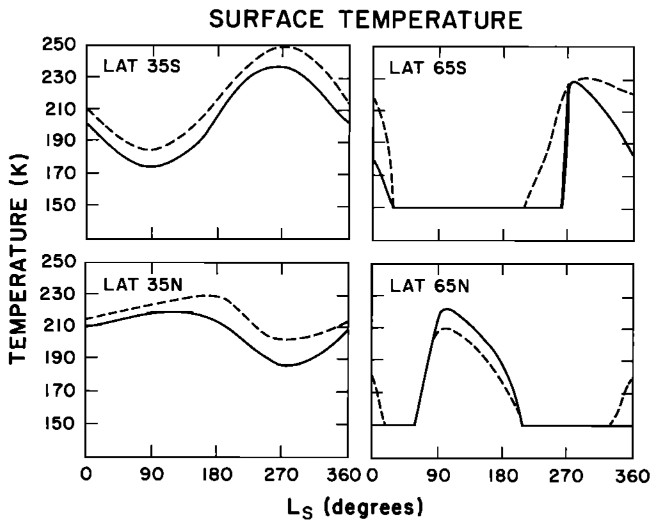

Fig. 2. Calculated mean surface temperature as a function of solar longitude for different latitudes. Solid curves represent the results of *Kieffer et al.* [1977] and dashed curves the present work.

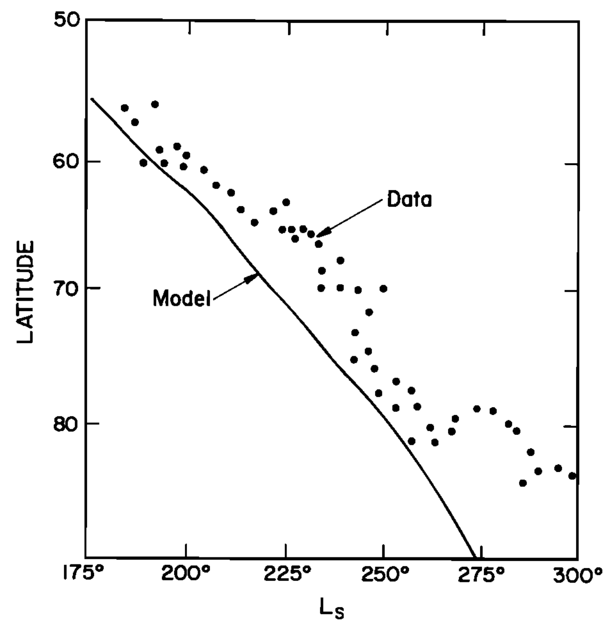

Fig. 3. Seasonal recession of the southern polar cap as predicted by the model. Data representing the maximum extent of the cap over 20 years are from *James and Lumme* [1982].

discrepancy can be partly explained by the fact that the model assumes a pure CO_2 polar ice rather than a mixture of CO_2 ice, water ice and clathrate. Another inaccuracy in the model is the surface elevation in the polar regions. Surface elevation is important for the estimation of the CO_2 saturation temperature and consequently affects the amount of CO_2 that condenses or sublimes at the surface. Accurate data on the surface elevation in the polar regions are not available and the zonally averaged topographic profile presented by *Mutch et al.* [1976] is used. Finally, the model does not include the effect of dust, which affects the radiative budget of the atmosphere, the albedo in the polar regions, and consequently the radiative exchanges at the surface.

Atmospheric Temperature and Circulation

In the Martian atmosphere, the temperature distribution varies mainly with season, latitude, solar activity and atmospheric dust content. The radiative heating of the clear atmosphere is primarily due to the radiative action of CO_2 and ozone bands. The strongest cooling in a clear atmosphere is due to the 15-μm band of carbon dioxide [*Lindner*, 1988]. In a dusty atmosphere, however, the dust cooling integrated over all wavelengths is appreciable and cannot be neglected compared to the cooling by the 15-μm band of carbon dioxide. Temperature data for the lower atmosphere (below 40 km altitude) have been provided by the Mariner 9 Iris [e.g., *Conrath,* 1981] and Viking IRTM [*Kieffer*, 1979] experiments. Viking landers, radio occultation techniques and the Soviet Mars 6 spacecraft [*Kerzhanovich,* 1976] have also provided a limited number of observations of the temperature fields for the upper part of the atmosphere. Using ground-based laser heterodyne spectroscopy, *Deming et al.* [1986] have shown that near subsolar latitudes the temperature in the altitude range 50–80 km is close to the radiative equilibrium for a pure CO_2 atmosphere but that at high latitudes, both in summer and winter, the 50– to 80–km temperature exceeds the radiative equilibrium temperature by more than 40 K.

The meridional distribution of temperature obtained by solving the thermodynamic equation in which radiative transfer and transport of heat are explicitly included is shown in Figures 4*a* and 4*b* for late northern winter conditions (Figure 4*a*) and northern summer solstice (Figure 4*b*). The basic features of the observed thermal field are well reproduced by the model. For the northern winter simulation corresponding to a solar longitude of 351° (Figure 4*a*), it is clear from the figure that an important meridional gradient of temperature exists, with the winter polar regions below about 30 km altitude exhibiting the lowest temperatures, in good agreement with the available data. The temperature profile in these regions is nearly isothermal up to 30 km altitude. In the middle atmosphere, above 35 km altitude, a temperature maximum occurs at polar latitudes. The temperature minimum, observed between southern and northern mid-latitudes in the middle atmosphere, is also well reproduced. In the lower atmosphere (below 35 km altitude), however, the calculated temperatures are lower than observed by the Mariner 9 IRIS experiment [e.g. *French and Gierasch*, 1979; *Conrath*, 1981]. Temperature data obtained by the IRIS experiment were obtained after a global dust storm, while the model neglects these effects. Figure 4*b* presents the calculated thermal field for northern summer solstice conditions (L_S = 83°). The distribution is characterized by a pronounced reverse meridional gradient of temperature between equatorial and polar latitudes in the middle atmosphere. In the equatorial regions, middle atmosphere temperatures are slightly lower than for L_S = 351°. Southern polar latitudes are in the polar night, so that the atmospheric temperatures in the lower atmosphere drop rapidly and exhibit a nearly isothermal profile (about 150 K) below 30 km altitude.

In order to understand the cause of a temperature maximum near 40 km altitude in the polar regions, the model has been run with CO_2 being the only radiatively active constituent. This simulation shows that absorption by ozone and water cannot explain the heating in this region of the atmosphere. This local warming appears therefore to be dynamical by essence and to result from compressional heating associated with downward residual mean motions which are forced by momentum drag resulting from gravity wave breaking. Recent studies [*Barnes*, 1990] have shown that breaking gravity waves may play an important role in the circulation of the middle atmosphere and in the temperature structure. The adiabatic expansion produced by the rising branch of the Hadley cell induces the minimum of temperature reproduced by our model near 30 km altitude. The transformed Eulerian mean circulation calculated for a solar longitude of 351° is shown in Figure 4*c*.

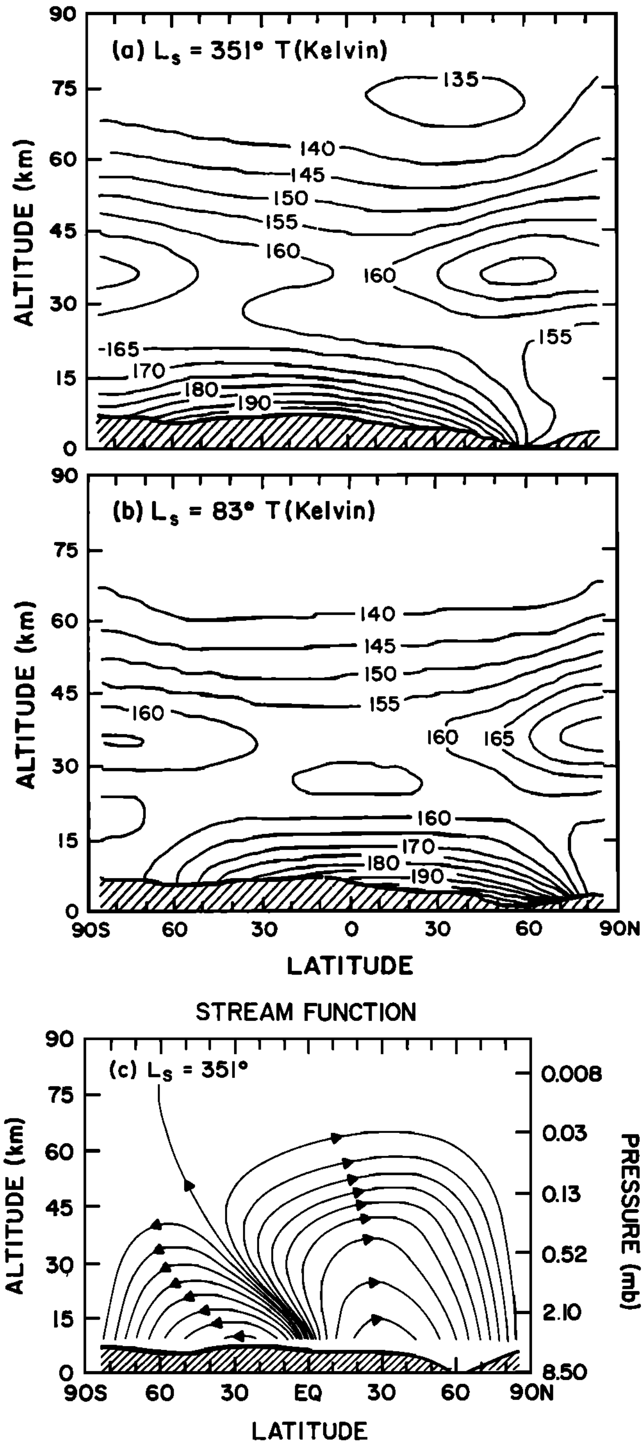

Fig. 4. Temperature distributions calculated for solar longitudes (*a*) L_S = 351° and (*b*) L_S = 83°. (*c*) The meridional circulation is calculated for L_S = 351°.

This figure suggests that the meridional transport of heat and trace gases is directed from the equator to the pole. The meridional velocity calculated for this period of the year reaches a maximum of 1.6 m s^{-1} at 50 km and 45°N latitude. The downward vertical velocity is largest over the polar regions and reaches 12.8 mm s^{-1}; it produces a substantial adiabatic heating in winter.

Some theoretical studies [*Haberle et al*, 1982] have also shown an increase of temperature during periods of global dust storms. This heating strongly affects the atmospheric circulation [*Haberle et al,* 1982] and consequently the structure of internal gravity waves. An increase in momentum drag by gravity waves should be expected and enhance the magnitude of the reversed meridional temperature gradient in the middle atmosphere.

Chemistry

The zonally averaged distribution of selected trace constituents will now be presented for solstice and equinox conditions.

Water vapor and odd hydrogen compounds. As indicated by previous studies [e.g., *Parkinson and Hunten,* 1972], the chemical composition of the Martian atmosphere is highly sensitive to the distribution of water vapor. The surface of Mars is a source of water during spring and summer and becomes a sink during fall and winter. Since these exchange processes are not accounted for in this study, several simple models of the water vapor distribution have been considered. The first of these models (model 1) is designed to reproduce the water vapor column abundance measured by Viking [*Jakosky and Farmer,* 1982]. These observations show that the water vapor abundance varies significantly with latitude and season, with values ranging from 3 to 20 precipitable microns at the equator (1 precipitable micron of water is equivalent to a column of 3.3 10^{18} molecules cm^{-2}) to as much as 90 precipitable microns at high latitude in mid summer. The water vapor column is lowest in winter: it drops drastically during the approach of the polar night in both hemispheres. To account for these variations with latitude and season, the water vapor density is assumed to decrease with altitude, with a scale height (5.385 km) equal to the half of the Martian atmospheric scale height (10.77 km). This assumption is intermediate between the suggestion by *Schorn et al* [1969] and *Hess* [1976] that water is probably concentrated near the surface, and with the study of *Davies* [1979] which suggests that the distribution of water vapor should be nearly uniform. The adopted surface concentration is chosen to reproduce the observed column abundance. Figures 5*a* and 5*b* show the meridional distribution for solar longitudes L_S = 351° (Figure 5*a*) and L_S = 83° (Figure 5*b*). In both cases the abundance of water vapor is substantially depleted over the polar caps.

In the second water vapor model (model 2), the same boundary conditions are used at the surface, but in this case the water mixing ratio is explicitly calculated, based on the photochemical and transport schemes developed in the model. This model emphasizes the role of photodissociation processes and meridional transport but neglects thermodynamic mechanisms such as possible saturation and condensation of water. Figure 6 shows the calculated distribution for L_S = 351°. In order to perform sensitivity analyses, model 3 is defined to be the same as model 1 but with a water vapor column chosen to be twice as large. Finally, model 4 assumes a mixing ratio constant with altitude. In this latter case the lower boundary condition is adjusted to fulfill the constraint on the observed column abundance.

Odd hydrogen constituents play a key role in the photochemical stability of the Martian atmosphere. They catalyze several mechanisms such as the recombination of CO and O to reproduce CO_2 [see *McElroy and Donahue,* 1972; and *Parkinson and Hunten,* 1972]. The production of odd hydrogen is mainly due to the photolysis of H_2O, the reaction of H_2O

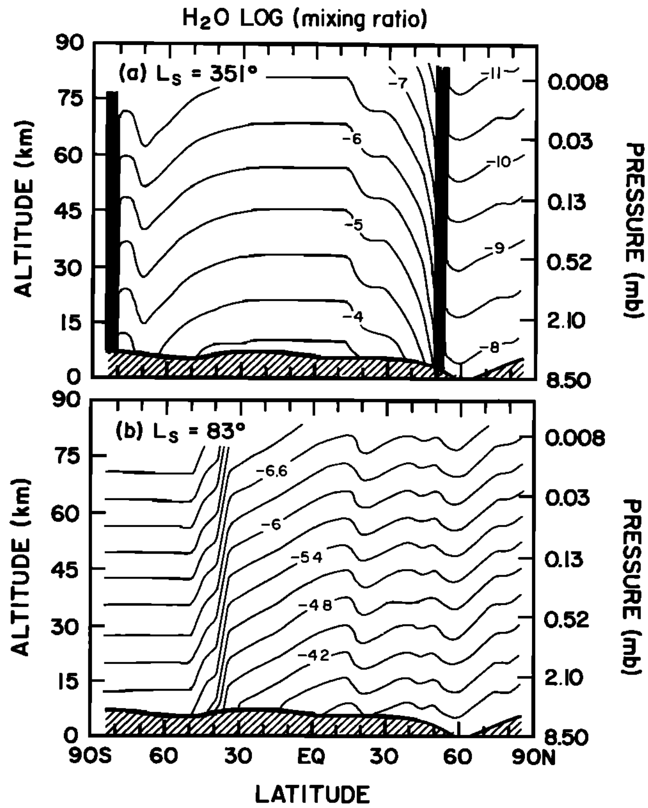

Fig. 5. Meridional distribution of the water vapor mixing ratio adopted as model 1 for solar longitude (*a*) L_S = 351° and (*b*) L_S = 83°.

with O(^{1}D), and that of H_2 with O(^{1}D). The latter is particularly important in a dry atmosphere. In the lower atmosphere the production of odd hydrogen by photodissociation of H_2 is slower than the reaction of molecular hydrogen with the electronically excited atomic oxygen. The photodissociation process, however, becomes important in the upper atmosphere and produces a downward flux of atomic hydrogen. Meridional contours of the number density for the hydroxyl radical calculated for model 1 of water vapor and for a solar longitude L_S = 351° are shown in Figure 7. Below 35 km altitude, the spatial variation of OH is correlated with the distribution of water which is controlled by condensation at low temperature. The maximum 24-hour averaged concentration is found near 40 km altitude.

Odd oxygen compounds. The formation of odd oxygen (O_3 and O) in the Martian atmosphere results from the photolysis of CO_2 and O_2; its destruction results from the recombination of O and O_3 which is catalyzed by the presence of hydrogen and nitrogen radicals (though the effect of odd nitrogen turns out to be relatively insignificant). The first measurement of ozone in the Martian atmosphere was made in 1969 by the Mariner 7 ultraviolet spectrometer which observed a column abundance of 10 μm-atm over the south polar cap [*Barth and Hord,* 1971]. (A micrometer-atmosphere is the thickness of the ozone column in micrometers when compressed to standard pressure and temperature on Earth; 1 μm-atm = 2.689 10^{15} molecules per square centimeter.) Two years later, during almost half of Martian year and two complete seasons for each hemisphere, the Mariner 9 ultraviolet spectrometer provided additional data on the latitudinal and seasonal variation of the ozone amount [*Barth et al.,* 1973; *Lane et al.,* 1973; *Barth and Dick,* 1974; *Barth,* 1985]. These observations suggest that significant

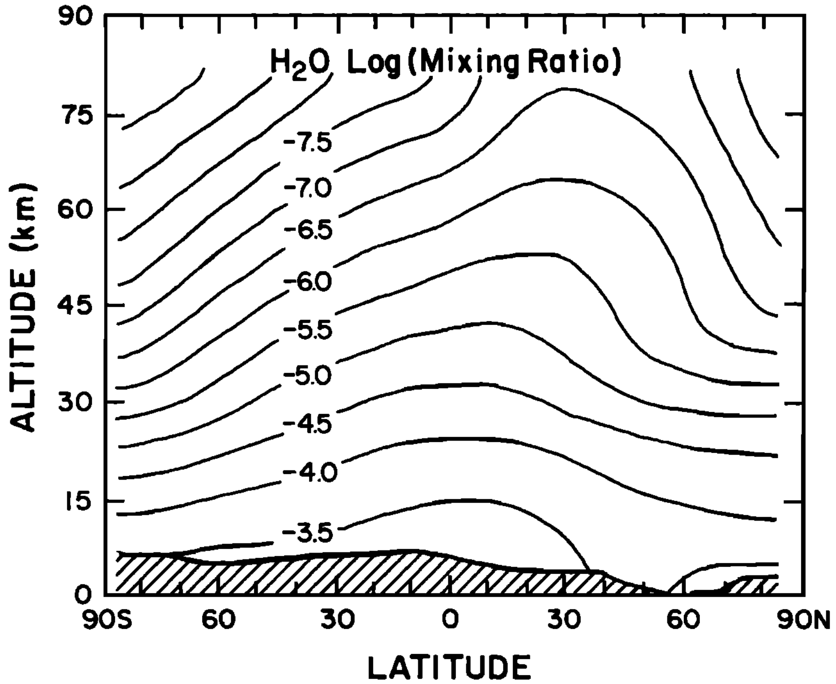

Fig. 6. Zonally averaged mixing ratio of water vapor calculated for $L_S = 351°$ (model 2).

amount of ozone are present poleward 40° latitude in the vicinity of the polar hood (a fog or cloud bank of water ice crystals). These findings led *Barth et al.* [1973] to suggest that ozone appears in early fall, together with the polar hood, reaches its maximum amount in winter when the extension of the polar hood is greatest and decrease monotonically to nearly disappear in early summer.

Integrated column densities generated by the model as a function of latitude for late winter conditions in the northern hemisphere are shown in Figure 8, for the different models of water vapor. The model predicts an ozone column at low and mid-latitudes which is consistent with the very low abundances found by Mariner 9. An increase in the ozone column abundance is found north of 40°N, but it is less pronounced in

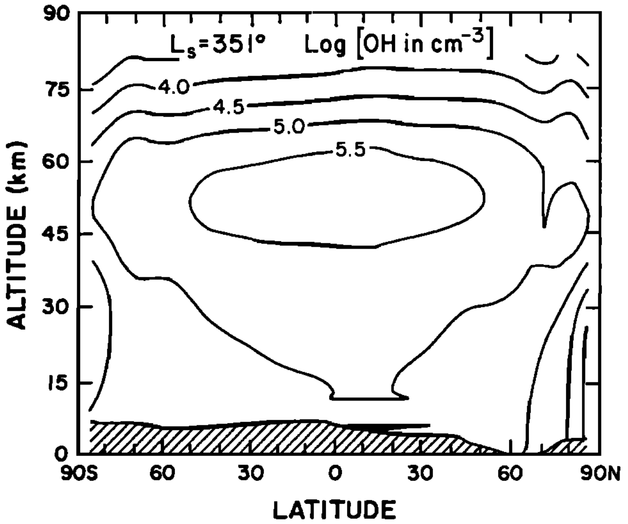

Fig. 7. Meridional distribution of the OH density calculated for $L_S = 351°$ and using water vapor shown in Figure 5*a* (model 1).

the model than the observations seem to indicate. The peak concentration found near 60°N is due to the low density of water vapor at these latitudes during winter. The decrease of the ozone amount at latitudes higher than 60° results from the decrease of the CO_2 photodissociation rate at large solar zenith angles. The behavior of ozone near the pole in winter is also sensitive to transport by the meridional circulation and to eddy mixing. The low concentration of O_3 at mid- and low latitudes results from the high water vapor densities in these regions and, consequently, to the efficient destruction of ozone by odd hydrogen catalytic cycles. The vertically integrated concentration of ozone calculated as a function of latitude and season (in the case of model 1) is compared in Figure 9 to the column of water vapor used in model 1 (Viking observations). There is clearly an anticorrelation between these two variables. At solar longitude $L_S = 351°$, for example, the water vapor abundance is highest in the tropics, where the ozone concentration is smallest. The ozone column is maximum at high latitude in winter, when the water vapor is small because of its condensation in the polar caps.

The calculated meridional distributions of ozone and atomic oxygen are shown in Figure 10 when model 1 is adopted for water vapor. Near the surface, the ozone concentration reaches a maximum of 1×10^{11} cm^{-3} at 60°N, but is significantly smaller at lower latitudes. Above 35 km altitude, the ozone concentration is almost independent of latitude. The spatial distribution of ozone below 35 km may be attributed to a combination of several factors. The latitudinal variation is determined by spatial variations in the distribution of water vapor. The large variations in the Martian topography and hence in surface pressure also affect the production, loss and therefore the concentration of ozone near the ground. The meridional distribution of atomic oxygen for the same seasonal conditions as in Figure 5*a* is shown in Figure 10*b*. The destruction of atomic oxygen occurs mainly below 35 km altitude where its concentration is controlled by HO_X

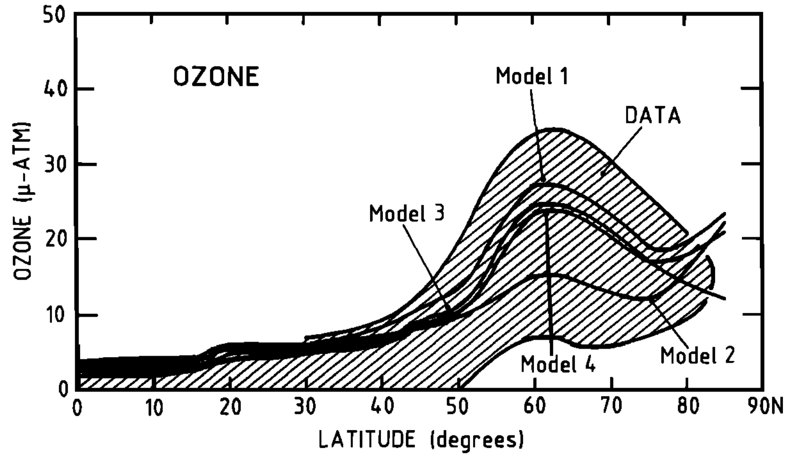

Fig. 8. Zonally averaged ozone column abundance as a function of latitude for the different water vapor distributions. Solar longitude is 351°.

compounds and by its recombination to form molecular oxygen. At higher altitude, the decrease in the atmospheric density and HO_x concentrations, as well as the downward flux of O associated with the CO_2 photolysis induce a maximum of concentration near 75 km altitude. The 24-hour averaged number density of the electronically excited oxygen atom is presented in Figure 11 for the same seasonal conditions as in

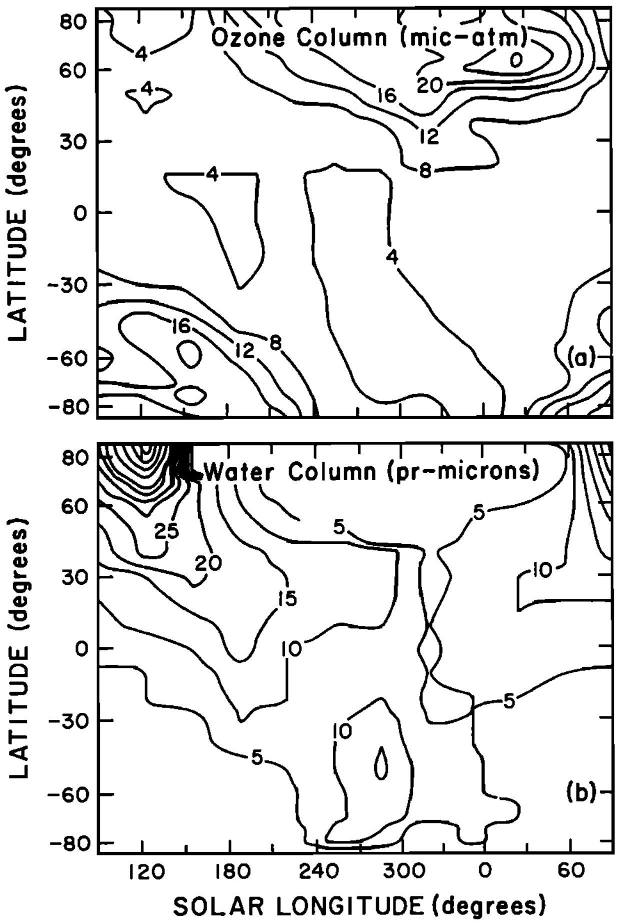

Fig. 9. (*a*) Calculated ozone column abundance (μm-atm) as a function of season and latitude compared to the (*b*) water column (μm precipitable water) used in the model.

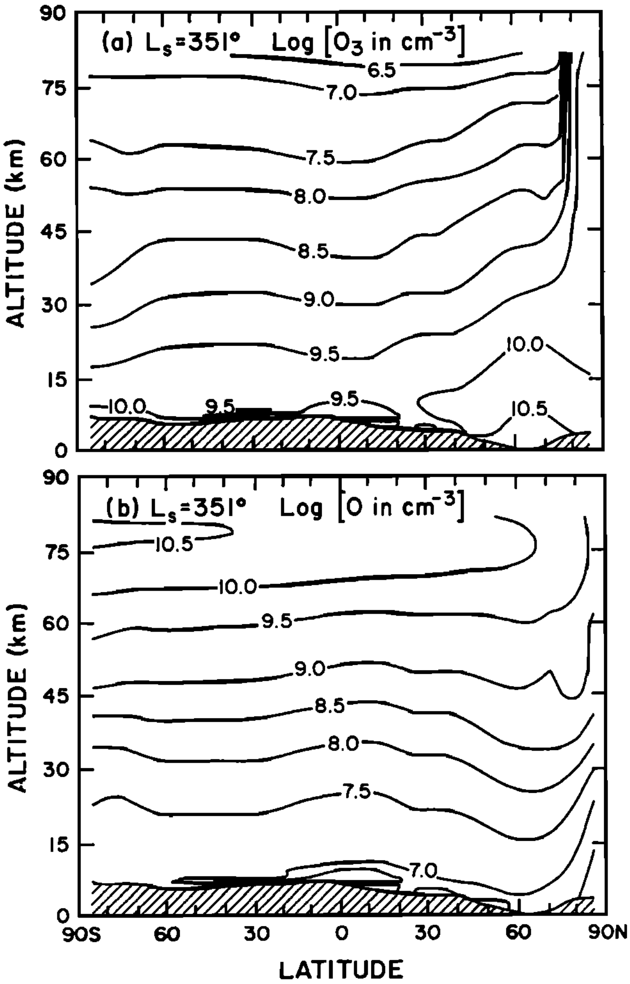

Fig. 10. Zonally averaged distribution of (*a*) ozone and (*b*) atomic oxygen concentrations for L_s = 351° and for model 1 of water vapor.

Figure 10. $O(^1D)$ reaches a maximum near 25 km altitude at mid-latitudes. The source of $O(^1D)$ atoms in the lower atmosphere is the photodissociation of ozone by solar ultraviolet radiation with wavelengths shorter than 320 nm. In the upper atmosphere, $O(^1D)$ is formed by CO_2 and O_2

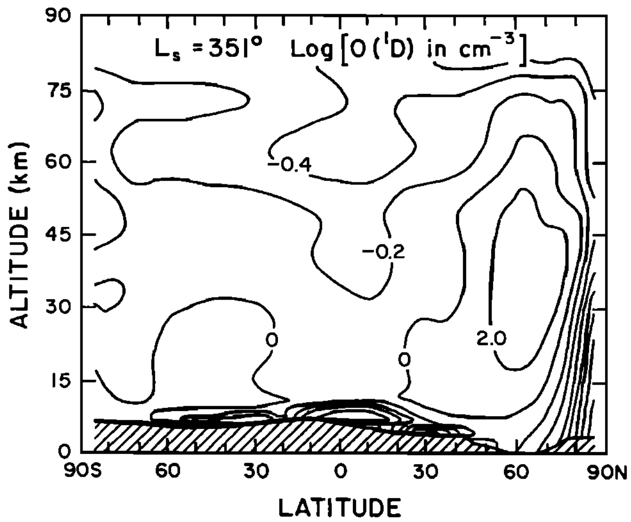

Fig. 11. Zonally averaged distribution of $O(^1D)$ concentration for the same conditions as Figure 10.

photodissociation. $O(^1D)$ is rapidly deactivated by collisions with the most abundant atmospheric constituents (reactions 2 to 8 in Table 2*a*). These reactions are very rapid and lead therefore to the very low calculated number densities. The enhancement of the $O(^1D)$ density near 60 km altitude over northern latitudes is due to the larger concentrations of ozone present in this altitude range (see Figure 10*a*).

Nitrogen compounds. The first calculations of nitrogen photochemistry in the Martian atmosphere were accomplished by *Sagan et al.* [1965], who found very low abundances of nitrogen oxides, followed in the late 1970s by the work of *Yung et al.* [1977] and *McElroy et al.* [1976, 1977]. Because the amount of nitrogen in the atmosphere of Mars is low, the contribution of NO_X chemistry on compounds belonging to the O_X and HO_X families is insignificant. The introduction of the nitrogen chemistry, however, is required to produce a comprehensive description of the chemical processes involved. The main source of odd nitrogen in the upper atmosphere results from the dissociation and dissociative ionization of N_2 by electron impact. The most important source of odd nitrogen in the lower atmosphere is due to the reaction of N_2O and $O(^1D)$. The loss of odd nitrogen occurs through predissociation of NO in the delta bands followed by recombination of N with NO. Another loss mechanism is the reaction between N and NO_2, which produce N_2O. Different transfer processes occur inside the odd nitrogen family and involve the presence of ozone, hydroxyl radicals and solar radiation. They lead to formation and destruction of NO, NO_2, NO_3, N_2O_5, HNO_2 and HNO_3. Figures 12*a* to 12*d* present contour plots of the calculated 24-hour averaged distributions of the nitrogen species NO, NO_2, HNO_3, and N. Over a wide range of altitudes, NO is the most abundant nitrogen species.

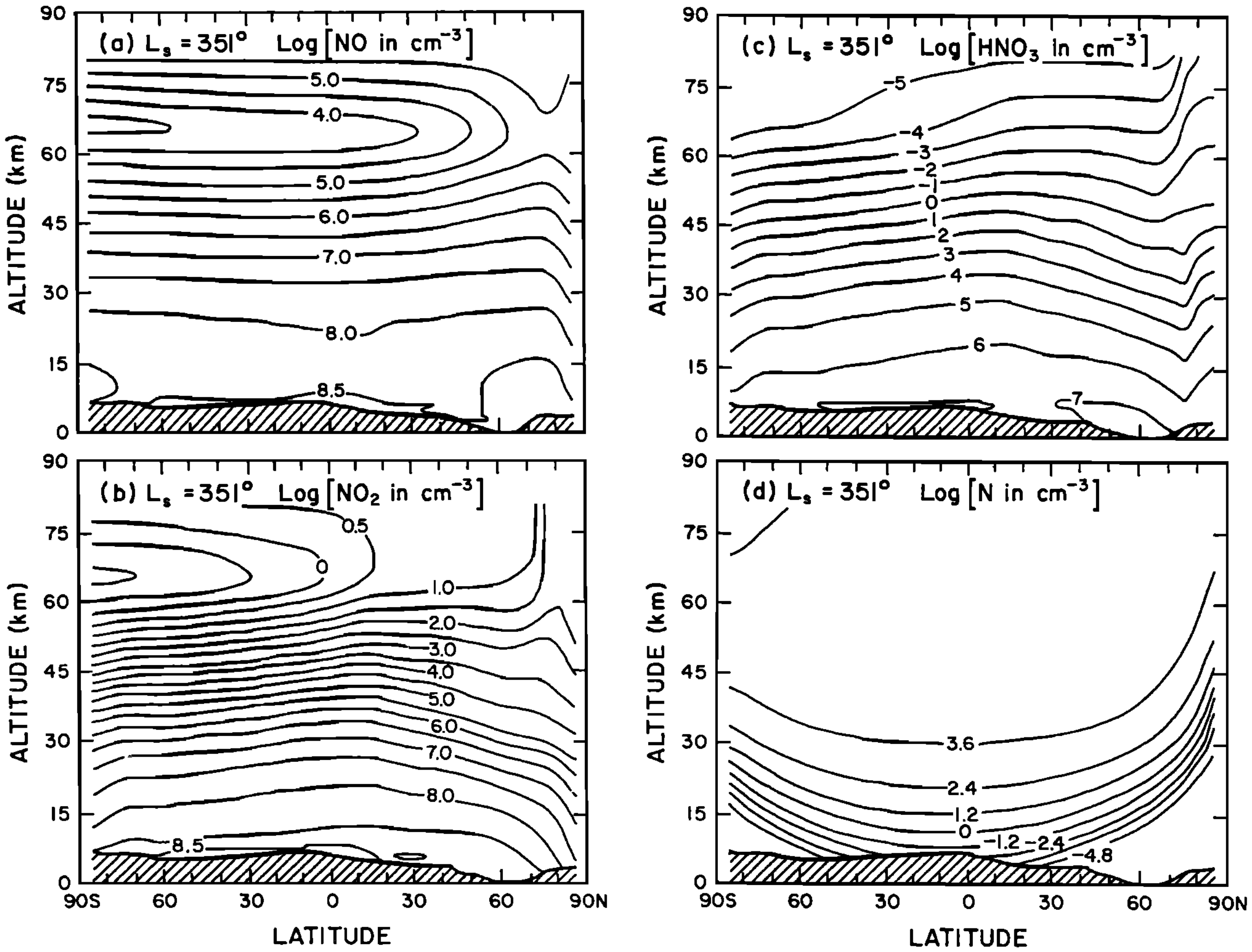

Fig. 12. Meridional distribution of (*a*) NO, (*b*) NO_2, (*c*) HNO_3, and (*d*) N number densities for the same conditions as in Figure 10.

Its concentration increases, above 60 km altitude, together with that of atomic nitrogen. Figure 12*b* shows the meridional distribution of nitrogen dioxide. NO_2 is the second important nitrogen constituent. Its formation results primarily from the reaction of NO with ozone and HO_2 and from reaction 56. The highest concentrations are found near the surface where ozone and HO_2 number densities are highest. Nitrogen dioxide is mainly destroyed by photodissociation and through reaction 30. Nitrogen dioxide reacts with OH to form nitric acid. HNO_3 is mainly removed by photodissociation. Figure 12*c* shows the latitudinal distribution of nitric acid. The highest number densities are found near the surface where high pressures ensure a more effective formation through the three-body reaction 58. Increase of the photodissociation rate with altitude as well as decrease of atmospheric density lead to the decrease of HNO_3 mixing ratio with altitude. Finally, the meridional distribution of atomic nitrogen is presented in Figure 12*d*. The presence of this constituent is associated with the NO photolysis. The lowest concentrations of N are found near the surface where N recombines rapidly with CO_2. It is interesting to note that the photolysis of nitric oxide leads to a minimum mixing ratio of NO near 65–70 km, which is most pronounced in summer. Through this photolytic process, there is thus a strong isolation between odd nitrogen produced by ionospheric processes in the upper atmosphere and by other mechanisms in the lower atmosphere. There is, however, a significant downward transport by the residual circulation of odd nitrogen from high altitudes in the polar night regions. This flux, which varies with dynamical conditions and solar activity could link the ionospheric production regions to the lower atmosphere at high latitudes and even lead to the deposition of nitrogen compounds in the ice polar caps during winter.

CONCLUDING REMARKS AND FUTURE WORK

The purpose of this paper was to present the formulation and the first results of an interactive chemical-dynamical-radiative two-dimensional model of the Martian atmosphere. Despite the simple formulation of dynamical processes, the temperature structure calculated with the present model is in fair agreement with observations, including the Mariner 9 Iris data. This temperature distribution results from both radiative and dynamical processes. The high temperatures calculated in the polar regions are determined by compressional heating associated with the downward cell of the residual circulation. The computed distributions of chemical species are consistent with the few available observations. An important unknown is the vertical distribution of atmospheric water vapor. An estimate of the exchange of water between the atmosphere and the surface needs to be performed by a detailed thermodynamic model before a more accurate analysis of the ozone budget can be achieved. Many factors play a key role in this cycle: adsorption/desorption in the subsurface regolith, atmospheric transport, condensation and sublimation at the surface and in the atmosphere, polar cap trapping. The model calculations presented here show that ozone is highly sensitive to water vapor and therefore to the cycle affecting this latter constituent. Calculated distributions of nitrogen species are in fairly good agreement with those calculated by *Yung et al.* [1977] and with the upper limits quoted by *Owen and Sagan* [1972]. The role of nitrogen species in the ozone budget is relatively insignificant.

The present study will be followed by the development of a more comprehensive model including the radiative and chemical effects of dust, clouds, polar hood and the global effect of the regolith. Dust, which is injected in the atmosphere during storms, at regional and global scales, can reach altitudes as high as 30–40 km. It plays a major role in the radiative transfer and chemistry of the Martian atmosphere. A coupled chemical, dynamical, radiative model for these storm conditions is currently being developed and will be presented in a forthcoming paper.

Acknowledgment. Comments on this manuscript by Vladimir A. Krasnopolsky are gratefully acknowledged. We are grateful to D. Sanerib for typing the manuscript. This work was supported by the National Aeronautic and Space Administration through grant NAGW-389. The National Center for Atmospheric Research is sponsored by the National Science Foundation.

REFERENCES

Andrews, D. G., and M. E. McIntyre, Planetary waves in horizontal and vertical shear: The generalized Eliassen-Palm relation and the zonal mean acceleration, *J. Atmos. Sci.*, *33*, 2031–2020, 1976.

Barker, E. S., Detection of molecular oxygen in the Martian atmosphere, *Nature*, *238*, 447–448, 1972.

Barnes, J. R., Possible effects of breaking gravity waves on the circulation of the middle atmosphere of Mars, *J. Geophys. Res.*, *95*, 1401–1432, 1990.

Barth, C. A., Photochemistry of the atmosphere of Mars, in *The Photochemistry of Atmosphere: Earth, the Other Planets, and Comets*, edited by J. Levine, 476 pp., Academic, San Diego, Calif., 1985.

Barth, C. A., and M. L. Dick, Ozone and the polar hood of Mars, *Icarus*, *22*, 205–211, 1974.

Barth, C. A., and C. W. Hord, Mariner ultraviolet spectrometer: Topography and polar cap, *Science*, *173*, 197–201, 1971.

Barth, C. A., C. W. Hord, A. I. Stewart, A. L. Lane, M. L. Dick, and G. P. Anderson, Mariner 9 ultraviolet experiment: Seasonal variation of ozone on Mars, *Science*, *179*, 795–796, 1973.

Boyd, J. P., The noninteraction of waves with the zonally averaged flow on a spherical Earth and the interrelationships of eddy fluxes of energy, heat and momentum, *J. Atmos. Sci.*, *33*, 2285–2291, 1976.

Brasseur, G., and P. C. Simon, Stratospheric chemical and thermal response to long-term variability in solar UV irradiance, *J. Geophys. Res.*, *86*, 7343–7362, 1981.

Brasseur, G., M. H. Hitchman, S. Walters, M. Dymek, E. Falise, and M. Pirre, An interactive chemical dynamical radiative two-dimensional model of the middle atmosphere, *J. Geophys. Res.*, *95*, 5639–5655, 1990.

Briggs, G. A., The nature of the residual Martian polar caps, *Icarus*, *23*, 167–191, 1974.

Carleton, N. P., and W. A. Traub, Detection of molecular oxygen on Mars, *Science*, *179*, 795–796, 1972.

Connes, P., J. Connes, and J. P. Maillard, Atlas des spectres infrarouges de Venus, Mars, Jupiter, et Saturne, Centre National de la Recherche Scientifique, Paris, 1969.

Conrath, B. J., Planetary-scale wave structure in the Martian atmosphere, *Icarus*, *48*, 246–255, 1981.

Conrath, B., R. Curran, R. Hanel, V. Kunde, W. Maguire, J. Pearl, J. Pirraglia, J. Welker, and T. Burke, Atmospheric and surface properties of Mars obtained by infrared spectroscopy on Mariner 9, *J. Geophys. Res.*, *78*, 4267–4278, 1973.

Davies, D. W., The vertical distribution of Mars water vapor, *J. Geophys. Res.*, *84*, 2875–2880, 1979.

Deming, D., M. J. Mumma, F. Espenak, T. Kostiuk, and D. Zipoy, Polar warming in the atmosphere of Mars, *Icarus*, *66*, 366–379, 1986.

DeMore, W. B., D. M. Golden, R. F. Hampson, C. J. Howard, M. J. Kurylo, M. J. Molina, A. R. Ravishankara, and S. P. Sander, Chemical kinetics and photochemical data for use in stratospheric modeling, Evaluation No. 8, *JPL Publ. 87-41*, Jet Propulsion Laboratory, Pasadena, Calif., 1987.

Dickinson, R. E., Infrared radiative heating and cooling in the Venusian atmosphere, I, Global mean radiative equilibrium, *J. Atmos. Sci.*, *29*, 1531–1555, 1972.

Farmer, C. B., D. W. Davies, A. L. Holland, D. D. LaPorte, and P. E. Doms, Mars: Water vapor observation from the Viking Orbiters, *J. Geophys. Res.*, *82*, 4225–4248, 1977.

French, R. J., and P. J. Gierasch, The Martian polar vortex: Theory of seasonal variation and observations of eolian features, *J. Geophys. Res.*, *84*, 4634–4642, 1979.

Gierasch, P., and R. Goody, A study of the thermal and dynamical structure of the Martian lower atmosphere, *Planet. Space Sci.*, *16*, 615–646, 1968.

Haberle, R., C. Leovy, and J. Pollack, Some effects of global dust storms on the circulation of Mars, *Icarus*, *50*, 322–367, 1982.

Hanel, R. A., B. Conrath, W. Hovis, V. Kunde, P. Lowman, W. Maguire, J. Pearl, J. Pirraglia, C. Prabhakara, B. Schlachman, G. Levin, P. Straat, and T. Burke, Investigation of the Martian environment by infrared spectroscopy on Mariner 9, *Icarus*, *17*, 423–442, 1972.

Hess, S. L., The vertical distribution of water vapor in the atmosphere of Mars, *Icarus*, *28*, 269–278, 1976.

Hitchman, M. H., and G. Brasseur, Rossby wave activity in a two-dimensional model: Closure for wave driving and meridional eddy diffusivity, *J. Geophys. Res.*, *93*, 9405–9417, 1988.

Hogan, L. G., and D. S. Burch, A measurement of the rate constant for the reaction $O + O_2 + O_2 \longrightarrow O_3 + O_2$, *J. Chem. Phys.*, *65*, 894–900, 1976.

Holton, J. R., The role of gravity wave induced drag and diffusion in the momentum budget of the mesosphere, *J. Atmos. Sci.*, *39*, 791–799, 1982.

Hunten, D. M., and M. B. McElroy, Production and escape of hydrogen on Mars, *J. Geophys. Res.*, *75*, 5989–6001, 1970.

Jakosky, B. M., and C. B. Farmer, The seasonal and global behavior of water vapor in the Mars atmosphere: Complete global results of the Viking atmospheric water detector experiment, *J. Geophys. Res.*, *87*, 2999–3019, 1982.

James, P. B., and K. Lumme, Martian south polar cap boundary: 1971 and 1973 data, *Icarus*, *50*, 368–380, 1982.

James, P., and G. North, The seasonal CO_2 cycle on Mars: An application of an energy balance climate model, *J. Geophys. Res.*, *87*, 10271–10283, 1982.

Kaplan, L. D., J. Connes, and P. Connes, Carbon monoxide in the Martian atmosphere, *Astrophys. J.*, *157*, L187–L192, 1969.

Kaufman, F., and J. R. Kelso, M effect in the gas-phase recombination of O with O_2, *J. Chem. Phys.*, *46*, 4541–4543, 1967.

Kerzhanovich, V. V., Mars 6: Improved analysis of the descent module measurements, *Icarus*, *30*, 1–25, 1976.

Kieffer, H. H., Mars south polar spring and summer temperatures: A residual CO_2 frost, *J. Geophys. Res.*, *84*, 8263–8288, 1979.

Kieffer, H. H., T. Z. Martin, A. R. Peterfreund, B. M. Jakosky, E. D. Miner, and F. D. Palluconi, Thermal and albedo mapping of Mars during the Viking primary mission, *J. Geophys. Res.*, *82*, 4249–4291, 1977.

Kiehl, J. T., and T. Yamamouchi, A parameterization for absorption due to the A, B, and γ oxygen bands, *Tellus*, *37b*, 1–6, 1985.

Kiehl, J. T., R. J. Wolski, B. P. Briegleb, and V. Ramanathan, Documentation of radiation and cloud routines in the NCAR community climate model (CCM1), *NCAR Tech. Note*, *NCAR/TN-288+IA*, National Center for Atmospheric Research, Boulder, Colo., 1987.

Krasnopolsky, V. A., and V. A. Parshev, Ozone and photochemistry of the Martian lower atmosphre, *Planet. Space Sci.*, *27*, 113–120, 1979.

Kratz, D. P., and R. D. Cess, Solar absorption by atmospheric water vapor: A comparison of radiation models, *Tellus*, *37b*, 53–63, 1985.

Kuiper, G. P., Infrared spectra of planets, *Astrophys. J.*, *106*, 251–254, 1947.

Kuiper, G. P., *The Atmosphere of the Earth and Planets*, edited by G. P. Kuiper, University of Chicago Press, Chicago, 1952.

Lacis, A. A., and J. E. Hansen, A parameterization for absorption of solar radiation in the Earth's atmosphere, *J. Atmos. Sci.*, *31*, 118–133, 1974.

Lane, A. L., C. A. Barth, C. W. Hord, and A. I. Stewart, Mariner 9 ultraviolet spectrometer experiment: Observation of ozone on Mars, *Icarus*, *18*, 102–108, 1973.

Leovy, C., and Y. Mintz, Numerical simulation of the atmospheric circulation and climate of Mars, *J. Atmos. Sci.*, *26*, 1167–1190, 1969.

Lewis, J. S., and J. H. Carver, Temperature dependence of the carbon dioxide photoabsorption cross section between 1200 and 1700 Angstroms, *J. Quant. Spectrosc. Radiat. Transfer*, *30*, 297–309, 1983.

Lindner, B. L., Ozone on Mars: The effect of clouds and airborne dust, *Planet. Space Sci.*, *36*, 125–144, 1988.

Lindzen, R. S., Turbulence and stress owing to gravity wave and tidal breakdown, *J. Geophys. Res.*, *86*, 9707–9714, 1981.

Magalhaes, J. A., The Martian Hadley circulation: Comparison of "viscous" model predictions to observations, *Icarus*, *70*, 442–468, 1987.

McConnell, J. C., and M. B. McElroy, Odd nitrogen in the atmosphere, *J. Atmos. Sci.*, *30*, 1465–1480, 1973.

McElroy, M. B., and T. M. Donahue, Stability of the Martian atmosphere, *Science*, *177*, 986–988, 1972.

McElroy, M. B., T. Y. Kong, Y. L. Yung, and A. O. Near, Composition and structure of the Martian upper atmosphere: Analysis of results from Viking, *Science*, *194*, 1295–1298, 1976.

McElroy, M. B., T. Y. Kong, and Y. L. Yung, Photochemistry an evolution of Mars's atmosphere: A Viking perspective, *J. Geophys. Res.*, *82*, 4379–4388, 1977.

Mutch, T. A., R. E. Arvidson, J. W. Head III, K. L. Jones, and R. S. Saunders, *The Geology of Mars*, Princeton University Press, Princeton, N. J., 1976.

Nier, A. O., W. B. Hanson, A. Seiff, M. B. McElroy, N. W. Spencer, R. J. Duckett, T. C. D. Knight, and W. S. Cook, Composition and structure of the Martian atmosphere: Preliminary results from Viking 1, *Science*, *193*, 786–788, 1976.

Owen, T., and K. Biemann, Composition of the atmosphere at the surface of Mars: Detection of Ar-36 and preliminary analysis, *Science*, *193*, 801–803, 1976.

Owen, T., and C. Sagan, Minor constituents in planetary atmospheres: Ultraviolet spectroscopy from orbiting astronomical observatory, *Icarus*, *16*, 557–568, 1972.

Parkinson, T. D., and D. M. Hunten, Spectroscopy and aeronomy of O_2 on Mars, *J. Atmos. Sci.*, *29*, 1380–1390, 1972.

Pollack, J., R. Haberle, R. Greeley, and S. Iversen, Estimate of the wind speed required for particle motion on Mars, *Icarus*, *29*, 395–417, 1976.

Pollack, J., C. Leovy, P. Greiman, and Y. Mintz, A Martian general circulation experiment with large topography, *J. Atmos. Sci.*, *38*, 3–29, 1981.

Sagan, C., P. L. Hanst, and A. T. Young, Nitrogen oxides on Mars, *Planet. Space Sci.*, *13*, 73–88, 1965.

Sasamori, T., J. London, and D. V. Hoyt, Radiation budget of the Southern Hemisphere, *Meteorol. Mag.*, *13*, 9–23, 1972.

Schneider, E. K., Martian great dust storms: Interpretive axially symmetric models, *Icarus*, *55*, 302–331, 1983.

Schorn, R. A., C. B. Farmer, and S. J. Little, High-dispersion spectroscopic studies of Mars, III, Preliminary results of 1968–1969 water vapor studies, *Icarus*, *11*, 283–288, 1969.

Shemansky, D. E., CO_2 extinction coefficient 1700–3000 A, *J. Chem. Phys.*, *56*, 1582–1587, 1972.

Yung, Y. L., D. F. Strobel, T. Y. Kong, and M. B. McElroy, Photochemistry of nitrogen in the Martian atmosphere, *Icarus*, *30*, 26–41, 1977.

G. Brasseur, Atmospheric Chemistry Division, National Center for Atmospheric Research, P.O. Box 3000, Boulder, CO 80307.

L. W. Esposito and D. Moreau, Laboratory for Atmospheric and Space Physics, University of Colorado, Boulder, CO 80309.

(Received October 23, 1989;
revised July 30, 1990;
accepted November 15, 1990.)